THE JOURNAL OF PHYSICAL CHEMISTRY B
A JOURNAL OF THE AMERICAN CHEMICAL SOCIETY

pubs.acs.org/JPCB

Article

Effects of Ions and Small Compounds on the Structure of Aβ_{42} Monomers

Farbod Mahmoudinobar, Bradley L. Nilsson, and Cristiano L. Dias*

Cite This: *J. Phys. Chem. B* 2021, 125, 1085–1097

Read Online

ACCESS | Metrics & More | Article Recommendations | Supporting Information

ABSTRACT: Aggregation of amyloid-β (Aβ) proteins in the brain is a hallmark of Alzheimer's disease. This phenomenon can be promoted or inhibited by adding small molecules to the solution where Aβ is embedded. These molecules affect the ensemble of conformations sampled by Aβ monomers even before aggregation starts. Here, we perform extensive all-atom replica exchange molecular dynamics (REMD) simulations to provide a comparative study of the ensemble of conformations sampled by Aβ_{42} monomers in solutions that promote (i.e., aqueous solution containing NaCl) and inhibit (i.e., aqueous solutions containing *scyllo*-inositol or 4-aminophenol) aggregation. Simulations performed in pure water are used as our reference. We find that secondary-structure content is only affected in an antagonistic manner by promoters and inhibitors at the C-terminus and the central hydrophilic core. Moreover, the end of the C-terminus binds more favorably to the central hydrophobic core region of Aβ_{42} in NaCl adopting a type of strand−loop−strand structure that is disfavored by inhibitors. Nonpolar residues that form the dry core of larger aggregates of Aβ_{42} (e.g., PDB ID 2BEG) are found at close proximity in these strand−loop−strand structures, suggesting that their formation could play an important role in initiating nucleation. In the presence of inhibitors, the C-terminus binds the central hydrophilic core with a higher probability than in our reference simulation. This sensitivity of the C-terminus, which is affected in an antagonistic manner by inhibitors and promoters, provides evidence for its critical role in accounting for aggregation.

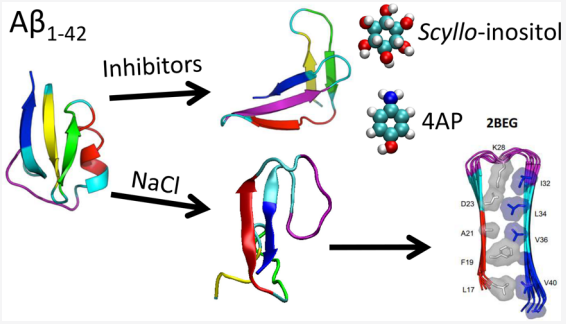

I. INTRODUCTION

The intrinsically disordered amyloid-beta (Aβ) protein is highly susceptible to aggregation and the formation of amyloid fibrils, which are the main constituent of senile plaques in the brain of Alzheimer's patients.[1−5] Rates of aggregation are affected by mutations in the Aβ sequence and properties of the solution in which the protein is embedded.[5−9] Faster aggregation rates are often related to increased cell toxicity, whereas inhibition of oligomer/fibril can be protective against Alzheimer's.[6,10−12] A signature of the aggregation propensity is expected to be encoded in the conformations of individual Aβ proteins, i.e., monomers.[13,14] In lattice models, specific monomeric structures were identified preceding fibril formation and the population of these structures under different conditions was found to correlate with the rate of fibril formation.[14] The existence of precursor monomeric Aβ structures could have important implications to treat Alzheimer's, as they could serve as targets for drugs aimed at reducing aggregation before the irreversible formation of fibrils.

Here, we use extensive all-atom molecular dynamics simulations in explicit solvent to perform a comparative study of Aβ conformations sampled under solvent conditions known to promote and inhibit fibril formation. Our goal is to identify monomeric Aβ conformations that are sampled more and less frequently under conditions that promote and inhibit aggregation, respectively. We anticipate that some of these conformations could be a precursor to aggregation and used as targets in the design of drugs to treat Alzheimer's. To represent conditions that favor aggregation, we use aqueous solutions containing NaCl at a concentration of 0.2 mM. Experimental studies have shown that NaCl can enhance aggregation by a factor of 3−4.[8] There are a large number of molecules that can inhibit aggregation. For the current study, we choose 4-aminophenol (4AP)[15] and *scyllo*-inositol[16,17] also at a concentration of 0.2 mM. The former has never been studied using all-atom simulations, and the latter has only been studied in the context of Aβ fragments.[18,19] They are also small in size which facilitates their computational study. Notice that other stereoisomers of inositol have been shown to have a lesser inhibiting effect on Aβ aggregation. As a reference, simulations are also performed in pure water. We find that secondary structure content does not change significantly in the different

Received: October 24, 2020
Revised: January 8, 2021
Published: January 22, 2021

https://dx.doi.org/10.1021/acs.jpcb.0c09617
J. Phys. Chem. B 2021, 125, 1085−1097

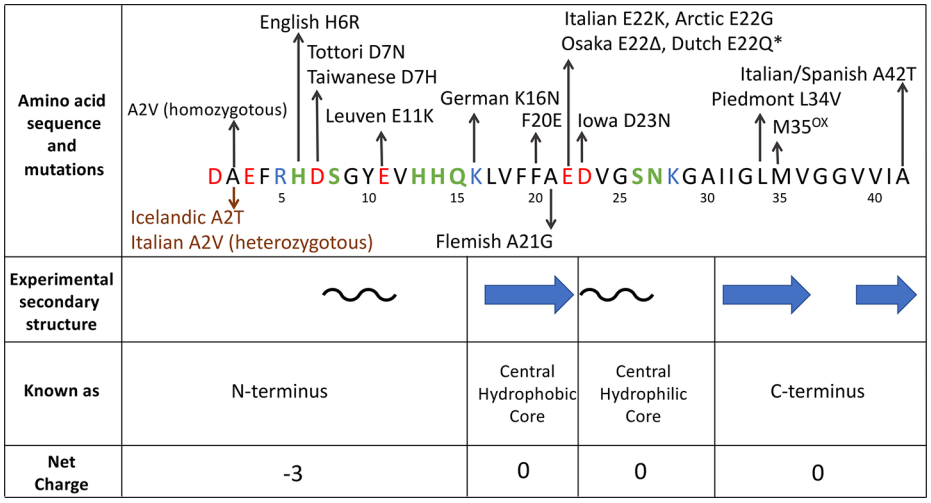

Figure 1. Amino acid sequence of Aβ_{42} and some of its point mutations associated with early onset Alzheimer's. Mutations are typically named after the geographic location in which they were first identified. Arrows pointing upward and downward represent mutations that increase and slow down Aβ aggregation, respectively. Brown color is used for mutations that are protective against Alzheimer's. Red, blue, and green colors in the Aβ_{42} sequence represent negative, positive, and polar residues, respectively. Experimentally identified turns and β-strands are marked using curled black lines and blue arrows, respectively. Residues comprising the N-terminus, central hydrophobic core, central hydrophilic core, and C-terminus are highlighted as well as the net charge of these regions. (References: A2T,[11] A2V,[11] D7H,[21] E11K,[22] K16N,[23] A21G,[24,25] E22G,[26] L34V,[27] A42T.[28,29])

solutions except at the C-terminus and the central hydrophilic core of Aβ. NaCl favors and discourages the formation of β-sheets at the C-terminus and central hydrophilic core, respectively. In contrast, β-sheets are discouraged by inositol at the C-terminus and favored by 4AP at the central hydrophilic core. There are also significant differences in how the end of the C-terminus interacts with the various Aβ regions in the different solutions. Interactions of the central hydrophobic core with the end of the C-terminus through the formation of antiparallel β-sheets are favored in the NaCl solution and inhibited in 4AP and inositol solutions. Interestingly, nonpolar residues that are close to each other in these β-sheets are found to be part of the dry core of a solid-state NMR model of Aβ_{42}, i.e., PDB ID 2BEG.[20] These structures may, therefore, play an important role in accounting for the increased nucleation rate of Aβ in NaCl solution. In 4AP and inositol solutions, the central hydrophobic core interacts preferentially with the central hydrophilic core.

This paper is organized as followed. First, we review current knowledge of monomeric Aβ structures obtained from experimental studies and all-atom computer simulations. This is followed by a discussion of small molecules and ions that are known to inhibit and promote aggregation, respectively. This includes a more detailed discussion of the effects of NaCl, *scyllo*-inositol, and 4AP on aggregation. In section I, the simulation method is described. Results are presented in section II followed by the discussion and conclusion in section III.

Structure of Aβ Monomers. The most abundant Aβ proteins in the brain of Alzheimer's patients are 40 and 42 residues long[30−33] with the latter, i.e., Aβ_{42}, exhibiting a faster aggregation rate and increased toxicity.[10,34] The Aβ sequence is commonly divided into four regions that have alternating hydrophilic−hydrophobic characters. Starting with the hydrophilic N-terminus (residues 1−16), the second, third, and fourth regions comprise residues 16−22, 23−29, and 30−42, respectively—see Figure 1. Compared to Aβ_{40}, the increased rate of aggregation of Aβ_{42} has been related to the more pronounced hydrophobic character of its C-terminus, which facilitates fibril nucleation while playing only a minor role on peptide solubility.[11,35]

The intrinsically disordered nature of Aβ implies that, under physiological conditions, monomers of this protein sample an ensemble of conformations without adopting a stable native structure.[36−38] In a recent comprehensive NMR study, this ensemble was shown to consist mainly of collapsed coil structures.[39] However, this study could not eliminate the possibility of monomeric Aβ adopting sparsely folded conformations with distinct structures. Accordingly, the measured hydrodynamic radius of the monomer is 0.9 nm, which characterizes relatively compact conformations as opposed to self-avoiding random structures.[40] In most NMR studies, hydrophobic regions of Aβ adopt β-strand conformations with the central hydrophilic region sampling turn motifs[13,37,41−43]—see Figure 1. This is consistent with the formation of transient strand−loop−strand conformations involving residues from the central hydrophobic core to the C-terminus.[44] Residues 7−11 have also been reported to form a β-strand in NMR studies[43]—see Figure 1. In agreement with these experiments, circular dichroism (CD) reported an overall β content of 24% for Aβ_{40} monomers[45] and Fourier transform infrared (FTIR) spectroscopy reported that these β-strands are packed in an antiparallel manner for monomeric and oligomeric states.[46,47] Notice that, since amyloid fibrils of Aβ are made of parallel β-sheets, a structural rearrangement has to take place during the nucleation of amyloid fibrils.

All-Atom Simulations of Aβ. Computer simulations have been providing important atomic level insights into the structure of Aβ monomers.[4,5,48−51] Earlier all-atom molecular dynamics simulations in explicit solvent reported a significantly lower frequency of β-strands compared to experiments. Recently, this discrepancy was shown to emerge in simulations where Aβ conformations are not sampled sufficiently.[13] It was shown that, in order to obtain equilibrium structural ensembles of Aβ monomers, extensive replica exchange molecular dynamics (REMD) simulations with over 400 ns of simulation

https://dx.doi.org/10.1021/acs.jpcb.0c09617
J. Phys. Chem. B 2021, 125, 1085−1097

per replica are necessary.[13,50] In these equilibrium molecular dynamics ensembles, β-strands are formed within the same residues as experiments and with a frequency close to the one measured experimentally. This result was reproduced using three force fields showing that equilibrium Aβ ensembles are mostly robust against changes in the force field.[13,51] Force fields were shown to affect mainly the flexibility of loop regions as well as electrostatic interactions between charged side chains, which appear to be overestimated in the OPLS-AA force field. These findings are reassuring and suggest that, when simulations are performed long enough to produce equilibrium ensembles, they can complement experiments by providing atomic level insights.

In computer simulations, structures of Aβ_{40} monomers are characterized by transient antiparallel β-hairpins between the central hydrophobic core and the beginning of the C-terminus (residues 30−34).[13] Transient contacts between the central hydrophobic core and the end of the C-terminus (residues 39−40 or 39−42), which are rare in Aβ_{40}, were also reported for Aβ_{42} monomers.[13,49,52] This may explain why the end of the C-terminus in Aβ_{42} is significantly more rigid and structured than in Aβ_{40}.[49,53,54] Double β-hairpins involving the central hydrophobic core and the beginning and the end of the C-terminus have also been observed for Aβ_{42} but not Aβ_{40}.[13,41,49] It was suggested that hydrophobic side chains in these double β-hairpins, which are exposed to the solvent, may serve as hot spots for self-aggregation.[41]

The effect of several point mutations on the structure of monomeric Aβ peptides has also been studied using computer simulations.[13,49,55,56] Mutations that reduce the net electrostatic repulsion between the negative N-terminus and negative residues at positions 22/23 accounted for a subtle increase in the bonding frequency of these regions with a rather small increase in the β-sheet character of the N-terminus. This included mutations in which the negative glutamic acid at position 22 was removed (Aβ_{40}−E22Δ), replaced with a positive lysine residue (Aβ_{40}−E22K), or replaced with glutamine (Aβ_{40}−E22Q) as well as mutations in which the negative aspartic acid at position 23 was replaced with asparagine (Aβ_{40}−D22N) or glycine (Aβ_{40}−E22G)[13,55]—see Figure 1. Mutation of alanine at position 2 with threonine (Aβ−A2T) is protective against Alzheimer's disease, and it reduces Aβ aggregation rates.[11,57] In one computational study, the Aβ_{42}−A2T mutation encouraged the N-terminus to interact with distant regions of the peptide.[56] This was related to a reduction in the population of double β-hairpins between the central hydrophobic core and the C-terminus, which are conformations that may precede fibril formation. However, in a more extensive study, the Aβ_{40}−A2T mutation was shown to affect the N-terminus in a similar fashion as the amyloidogenic mutations in residues 22/23. This raised the question of whether the effect of this mutation on the structure of monomers was responsible for its protective role in Alzheimer's.[13]

Inhibitors and Promoters of Aβ Aggregation. Motivated by the anticipated therapeutic effect of inhibiting Aβ aggregation, several studies have been dedicated to compounds that can produce this effect when added to the solution.[7,9,58−64] Examples of molecules that can inhibit Aβ aggregation include ibuprofen,[65,66] curcumin,[67] naproxen,[68] norepinephrine,[69] wgx-50 (extracted from Sichuan pepper),[70] and epigallocatechin gallate (EGCG), which is an abundant polyphenol in green tea.[71,72] A common feature of these molecules is the presence of at least one aromatic ring in their structure, suggesting their potential to disrupt hydrophobic and pi-stacking interactions between Aβ side chains. Similarly, 4-aminophenol (4AP)[15] and *scyllo*-inositol,[16,17] which will be studied in this work, also contain aromatic groups—see Figure 2. At concentrations above 10 μM, the former was shown to inhibit the formation of soluble Aβ oligomers as well as amyloid fibrils and to disrupt preformed aggregates.[15] Moreover, 4AP was shown to block Aβ toxicity in rat hippocampal neurons in cell culture. *scyllo*-Inositol was shown to inhibit fibril formation of Aβ_{42} at concentrations of 1−5 mM and to block toxicity of this protein in primary human neuronal cultures.[16] Interestingly, a different stereoisomer of inositol, i.e., *chiro*-inositol, did not have a significant effect on Aβ aggregation.

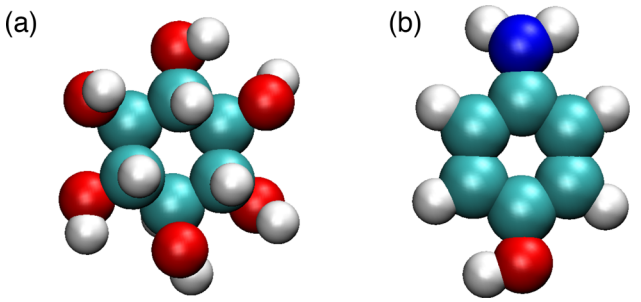

Figure 2. Atomic structures of (a) *scyllo*-inositol and (b) 4-aminophenol (4AP). Carbon, oxygen, nitrogen, and hydrogen atoms are shown in cyan, red, blue, and white spheres, respectively.

In contrast to inhibitors, some molecules can promote fibril formation. Examples are metal ions, i.e., Cu^{2+} and Zn^{2+}, which have a high affinity for the histidine-rich N-terminus of Aβ.[73,74] They are found in plaque regions of diseased brains where they may play a key role in the formation and stability of Aβ aggregates.[75,76] In the same vein, salts, e.g., NaCl, promote nucleation and growth of Aβ_{40} fibrils by reducing the lag phase and increasing the fibril growth rate, respectively. This accounts for amyloid fibrils forming 3−4 times faster in solutions containing NaCl at physiological concentrations, i.e.,150 mM.[8] These kinetic effects of amyloid fibrils were related to nonspecific shielding of electrostatic interactions[8,77] whereby reduced repulsion between monomers and fibril surfaces was shown to promote secondary nucleation events.[8] In one thorough study, effects of salt were attributed to specific ion−peptide interactions, changes in water structure (surface tension), and changes in the structure of the reaction product, i.e., Aβ aggregates.[78] The stability of amyloid fibrils also increases with increasing salt concentration.[78]

Most molecular dynamics studies have focused on understanding how small molecules bind to fibril models of Aβ (e.g., PDB ID 2BEG). These studies often highlight binding pockets of the fibril model and the hydrogen bonding network of the Aβ compound complex.[67−71,79] Fibrils and oligomers made from short segments of Aβ are also commonly used as targets for small compounds. Of particular interest to our work, *scyllo*- and *chiro*-inositol have been shown to interact predominantly via hydrogen bonds to models of $(GA)_4$ fibrils.[18] In another study, inositol was found to bind to monomers and disordered aggregates less efficiently than protofibrils of Aβ_{16-22}, with *scyllo*-inositol displaying a higher binding affinity for phenylalanine-lined grooves on the protofibril surface than *chiro*-

https://dx.doi.org/10.1021/acs.jpcb.0c09617
J. Phys. Chem. B 2021, 125, 1085−1097

inositol.[19] Aβ monomers have also been used as a binding target for compounds in a few computational studies. This is particularly relevant for the development of drugs which aim to stop aggregation before oligomers and stable fibrils have formed. It requires, however, extensive sampling of the conformational space due to the intrinsically disordered nature of Aβ. In one study, the *S*-isomer of ibuprofen was shown to bind more strongly to Aβ_{42} monomers than the *R*-isomer, which is consistent with experiments.[66] In another study, hexapeptides inspired by the N-terminus of Aβ that inhibit aggregation were shown to discourage the formation of contacts between the central hydrophobic core and the C-terminus.[80] Longer simulations than the ones performed so far are however required to account for conformational ensembles of Aβ in the presence of solutes that are independent of the initial structure.

II. METHODS

Conformations of Aβ_{42} monomers in pure water and aqueous solutions containing ~0.2 M NaCl, inositol, or 4-aminophenol (4AP) are studied. A helical conformation of Aβ_{42} (PDB ID 1IYT) was used as its initial structure in the simulations with zwitterionic termini and side chain protonation states appropriate for pH 7.[81] For simulations performed in pure water, the peptide is placed in a cubic box of 6 nm length containing 6305 TIP3P water molecules. The net charge of the box was neutralized by adding 3 Na^+ ions in the solution. Details of the simulation setup in the other aqueous solutions are summarized in Table 1. The AMBER99sb-ILDN force field

Table 1. Details of the Simulations Performed in This Study

	ns per replica	water molecules	solute molecules	concentration (in M)
water	600	6305	0	0
NaCl	700	6305	23	0.196
inositol	700	6305	23	0.193
4AP	700	6305	23	0.192

is used in all simulations, as it provides reasonable agreement with NMR data for small proteins and the Aβ peptide.[13,41,82−84] The energy of the system was minimized, and the system was equilibrated in the NPT ensemble (300 K and 1 atm) for 500 ps. Final conformations of this equilibration period were used to perform constant pressure replica exchange molecular dynamics (REMD) simulations.[85] In these simulations, the system was coupled to a velocity-rescaling thermostat (τ_T = 0.1 ps) to maintain a constant average temperature and the Berendsen barostat (τ_P = 0.1 ps) was used to maintain an average pressure of 1 atm. Periodic boundary conditions were applied, and the particle-mesh Ewald (PME) method was used to treat long-range electrostatic interactions. A 1.0 nm cutoff distance was used for van der Waals interactions and short-range electrostatic interactions. Covalent bonds were constrained using the LINCS algorithm, and an integration time step of 2 fs was used together with the leapfrog integrator. Simulations were performed using GROMACS version 5.1.[86]

REMD Simulation Details. We used 64 replicas with temperatures distributed exponentially in the 310−500 K range.[87] Swaps between replicas were attempted every 4 ps, which resulted in an average exchange probability of approximately 20%. Each system was simulated for 700 ns/replica, with the exception of simulations performed in pure water which converged faster and were simulated for 600 ns/replica. Convergence of the simulations was assessed by computing the secondary structure content of Aβ. We used the DSSP algorithm[88] to determine secondary structures of a given conformation. The overall secondary structure content of Aβ averaged over windows of 50 ns is shown in Figure 3.

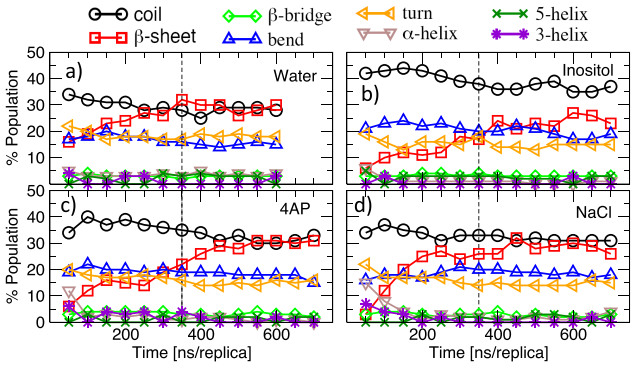

Figure 3. Convergence of REMD simulations at 320 K. Content of secondary structures for simulations performed in (a) water, (b) inositol, (c) 4AP, and (d) NaCl as determined by DSSP over 50 ns windows. Dashed lines show the threshold time above which secondary structures have converged.

Secondary structures converge after 400 and 500 ns for simulations performed in pure water and the other aqueous solutions, respectively. The last 200 ns of each ensemble at 320 K is used for all analysis and is referred to as a *production run*. The fluctuation in β-sheet content during the production run was less than 5%—see Figure 3 and Table 2. Notice that,

Table 2. Average Quantities Computed at 320 K[a]

	water	NaCl	inositol	4AP
β	31.5 ± 0.02	30.7 ± 0.01	27.5 ± 0.02	33.7 ± 0.01
helical	6.5 ± 0.01	4.5 ± 0.02	3.2 ± 0.03	2.5 ± 0.01
coil	28.7 ± 0.01	31 ± 0.01	36.5 ± 0.02	31 ± 0.01
R_g	1.03 ± 0.14	1.02 ± 0.13	1.07 ± 0.11	1.07 ± 0.13
N_{HB}	14.6 ± 3.2	13.4 ± 3.1	11.7 ± 3.0	13.6 ± 3.3
N_b		0.9 ± 0.23	13 ± 0.05	6 ± 0.06

[a]Helical, coil, and β contents are given in percentage. R_g and N_{HB} correspond to the radius of gyration (in nm) and number of intra-backbone hydrogen bonds, respectively. N_b corresponds to the average number of Na^+, Cl^-, inositol, or 4AP molecules bound to the Aβ_{42} surface. Uncertainties are estimated using standard deviation.

among the different types of secondary structures, β-sheets are the slowest to converge and could explain why simulations performed over short periods of time report low values of β-sheets.[41] In Figures S1 and S2 of the Supporting Information, we also show distributions of the radius of gyration (R_g), end-to-end distance (d_{ee}), number of backbone hydrogen bonds (N_{HB}), and solvent accessible surface area (SASA). These distributions which are computed for trajectories spanning the last and second-to-last windows of 100 ns do not change significantly and provide further evidence that equilibrium ensembles have been obtained.

***scyllo*-Inositol, 4AP, and NaCl.** Parameters for inositol and 4AP were obtained using AmberTools17 as follows: the electrostatic potentials of inositol and 4AP were obtained at

https://dx.doi.org/10.1021/acs.jpcb.0c09617
J. Phys. Chem. B 2021, 125, 1085−1097

the HF/6-31G* level after a geometry optimization at the AM1 level of theory. Partial charges were derived by fitting the electrostatic potential using the bond-charge correction (BCC) method, and the other force field parameters of the molecules were taken from the GAFF parameter set.[89] Force field details of inositol and 4AP used in this study are provided in section S2 of the Supporting Information. For NaCl, force field parameters defined by Joung et al. were employed.[90]

To define binding of *syllo*-inositol, 4AP, Na^+, and Cl^- molecules to the surface of $A\beta_{42}$, a distance cutoff of 0.4 nm is used. This cutoff is estimated from the distribution of the minimal distance of each molecule to the protein surface—see Figure S8.

III. RESULTS AND DISCUSSION

Average Properties. Table 2 shows mean values of different structural quantities of $A\beta_{42}$ computed during the production run. Regarding the content of secondary structures, the percentage of residues adopting β (i.e., β-sheet and β-bridge), helical (i.e., α-helix, 5-helix, and 3-helix), and coil structures in the pure water solution is 31, 6.5, and 29%, respectively. The experimentally measured β-sheet content of $A\beta_{40}$ monomers is 24%, which is close but lower than that in our simulations.[45] For the pure water solution, the average radius of gyration (R_g) of backbone atoms and the number of backbone hydrogen bonds is 1.03 nm and 14.6, respectively. This simulated R_g is consistent with the experimentally measured hydrodynamic radius of $A\beta_{42}$ which is 0.9 ± 0.1 nm.[40] These values for the radius of monomeric $A\beta_{42}$ are significantly lower than the one predicted for an unstructured protein (i.e., self-avoiding random walk structures of a 42-residue protein) which is 1.22 nm.[91] In summary, Table 2 suggests that the ensemble of monomeric $A\beta_{42}$ structures is largely disordered with some secondary structures forming along the sequence (mostly β-strands) and interacting with each other to account for conformations that are more compact than expected for an unstructured protein of the same size.

Average quantities of $A\beta_{42}$ in solutions containing NaCl or 4AP show only small differences when compared to the ones computed in pure water—see Table 2. Adding inositol to pure water accounts for $A\beta_{42}$ structures that are more disordered; i.e., they exhibit less β and more coil structures while being more swollen (i.e., displaying a higher radius of gyration) and forming less intrabackbone hydrogen bonds. This more pronounced effect of inositol on the conformational ensemble of $A\beta_{42}$ can be explain by its stronger binding to the protein surface. In Table 2, we show that the surface of $A\beta_{42}$ binds on average 13 inositol molecules as opposed to 6 for 4AP and less than 1 Na^+ ion and 1 Cl^- ion—see also Figures S6 and S7. These molecules bind nonspecifically to $A\beta_{42}$—see Figures S4 and S5. Notice that, despite coating the $A\beta$ surface, even inositol produces only small changes in the computed structural quantities when averaged over all residues—see Table 2. This may be explained by the degree of solvation of the protein which does not change significantly under the different conditions simulated—see Figure S8b. Thus, we will now focus on analyzing individual residues of $A\beta_{42}$.

Secondary Structures. Parts a and b of Figure 4 show the percentage of frames in which each $A\beta_{42}$ residue adopts β (panel a) or turn (panel b) conformations. We focus on these two types of secondary structures, as they are the main ones involved in fibril formation—see Figure S3 for the content of

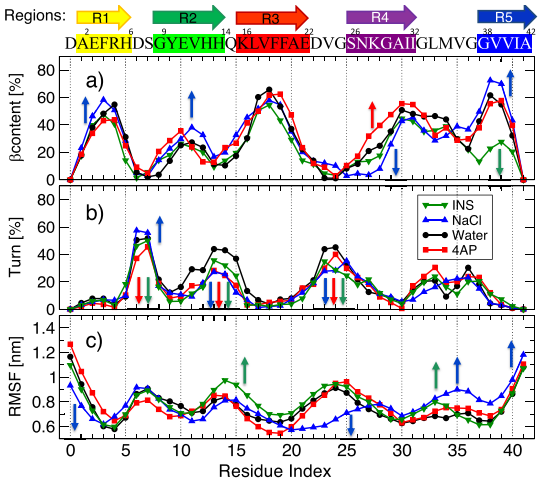

Figure 4. Secondary structure content and root mean squared fluctuation (RMSF) of each $A\beta_{42}$ residue at 320 K in inositol, NaCl, pure water, and 4AP. The amino acid sequence of $A\beta_{42}$ and the five regions with the highest amount of β-sheet are shown in the top panel. The average content of (a) β and (b) turn conformations, as defined using DSSP, is depicted for each residue. (c) The RMSF of backbone atoms for each residue is depicted. Arrows are used to highlight main changes with respect to simulations in pure water.

coil, bend, and α-helix for each residue. Four regions of $A\beta_{42}$ have a high propensity to form β conformations independently of the solvent. They are residues 2−6 and 9−14 of the N-terminus, residues 16−22 of the central hydrophobic core, and residues of the C-terminus. In addition, the β content is mainly affected by the type of solvent at residues 26−32 of the central hydrophilic core. These regions are chosen for further analysis in this paper. For simplicity, they are numbered sequentially (R1−R5), as shown in Figure 4. We choose residues 38−42 of the C-terminus to represent region R5, as these residues account for a high level of β-sheet content that varies significantly with the type of solution. Notice that residues in between two consecutive β-sheet regions exhibit a high probability to form turns (Figure 4b), suggesting the formation of β-hairpins in the simulation. Regions with high β content in Figure 4 are in agreement with other computational studies performed with different force fields.[13,41,51]

Compared to pure water, the presence of NaCl in the solution increases the probability of forming both β-strands at regions R1 and R2 as well as turns in residues located between these regions. This suggests the formation of a β-hairpin at the N-terminus. Charge screening by NaCl, which reduces the electrostatic repulsion between these negatively charged regions, is a possible mechanism for the preference of this β-hairpin. Also, NaCl increases and reduces the formation of β-strands in regions R5 and R4, respectively. A main effect of inositol is to significantly reduce the percentage of β-strands in region R5, whereas 4AP increases the percentage of β-structures in region R4. Inositol, 4AP, and NaCl reduce the formation of turns in residues located between regions R2−R3 and R3−R4. We use arrows in Figure 4 to highlight these changes.

RMSF. The flexibility of $A\beta_{42}$ residues is affected by the formation of β-strands and turns. This flexibility can be estimated by computing backbone root mean square fluctuation (RMSF). This quantity corresponds to the standard deviation of the backbone's atomic positions with respect to

https://dx.doi.org/10.1021/acs.jpcb.0c09617
J. Phys. Chem. B 2021, 125, 1085−1097

their average values. In Figure 4c, we show that the highest RMSF values occur for residues at both extremities of the protein where they are more free to move. The flexibility of residues in the middle of Aβ_{42} alternate between high (∼1.0 nm) and low (∼0.6 nm) RMSF values, which coincide with regions exhibiting high turn and β-strand content, respectively.

NaCl reduces the flexibility of the negatively charged N-terminus, and it increases the flexibility of the nonpolar C-terminus. Previously, Aβ_{42} regions with high flexibility were proposed to initiate aggregation, as they are more prone to move and interact with neighboring proteins.[55] The increased flexibility of the C-terminus in the NaCl solution may suggest such a role for this Aβ_{42} segment. Another region of the protein that is affected by NaCl is the central hydrophilic core comprising residues in region R4 that become more rigid. Inositol increases the flexibility of the central hydrophobic core of Aβ, i.e., region R3, and its adjacent residues involved in turn formation. In contrast, 4AP reduces the flexibility of region R3 and residues involved in turn formation between regions R1 and R2. To provide a better understanding of these changes, in the next section, we investigate the pair interactions of residues, i.e., contact map, in different solutions.

Contact Maps. Contact maps in Figure 5a,b assume that two residues are in contact when the distance between their C_α−C_α atoms is less than 8 Å. These maps are discussed in terms of the five regions introduced in Figure 4. In pure water, Aβ_{42} forms antiparallel contacts with a high probability between regions R1−R2 and R3−R4 and with a lower probability between regions R1−R5 and R4−R5. In the NaCl solution, we observe an increase in contacts between regions R1 and R2 consistent with the formation of a β-hairpin between these regions, as discussed in Secondary Structures section and Figure 4. Also, compared to Aβ_{42} in pure water, less contacts are formed between regions R3 and R4 and new antiparallel contacts are formed between regions R3 and R5. This suggests a shift in registry at region R3 whereby residues prefer to interact with the end of the C-terminus (i.e., region R5), instead of interacting with the neighboring region R4. This could explain the higher β-sheet content at region R5 in Figure 4 for the NaCl solution compared to pure water. All pairs of regions form significantly less contacts in the inositol solution than in pure water except for R1−R2 and R4−R5. In the solution containing 4AP, there is an increase in R3−R4 and R4−R5 contacts which suggests the formation of longer β-sheets made from three strands with region R4 in the middle.

To better illustrate effects of the solvent, we depict in Figure 5c,d differences in Aβ_{42} contact maps. In this figure, we highlight the main antagonistic effect of NaCl and inhibitors which occurs for contacts between regions R3 and R5. Contacts between these regions are scarce in pure water and almost nonexistent in solutions containing inhibitors, whereas they occur frequently and in an antiparallel fashion in the NaCl solution. Contacts between regions R4 and R5 are more pronounced in solutions containing 4AP and (to a lesser extend) inositol than in pure water, but these contacts are not significantly affected by NaCl. Changes in the frequency of contacts between other regions do not produce antagonistic effects for promoters and inhibitors of fibril formation. For example, contact frequencies between regions R1 and R2 increase in both NaCl and inositol solutions compared to pure water. In the same vein, a lower frequency of contacts is observed between regions R3 and R4 for both NaCl and inositol. A summary of these changes is provided in Table 3.

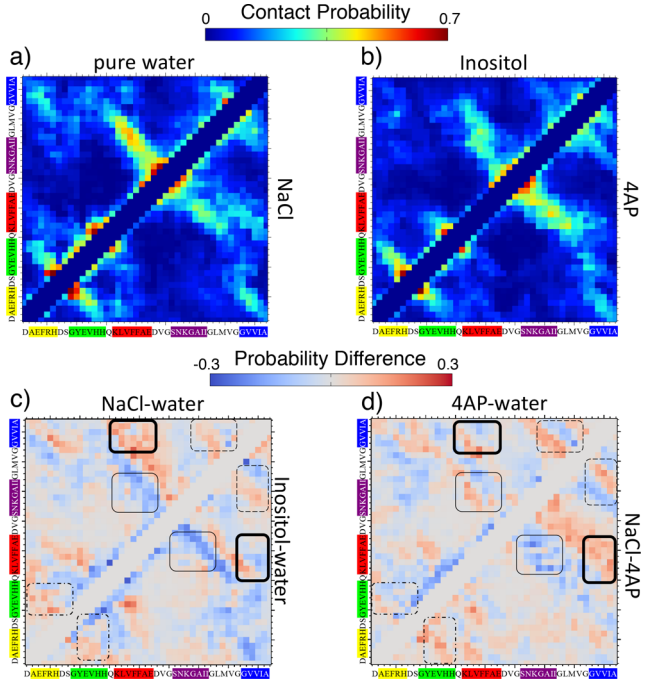

Figure 5. Contact maps of C_α atoms in (a) pure water and NaCl solution as well as (b) inositol and 4AP solutions. The color scheme corresponds to the contact probability computed over the production run. Only nonsequential contacts ($|i - j| > 3$) are shown in the maps. Contact map differences with respect to pure water for (c) NaCl (upper corner) and inositol (lower corner) as well as (d) 4AP (upper corner) are depicted. The lower corner of panel d corresponds to differences between NaCl and 4AP contact maps. Thick and thin rectangles correspond to contacts between regions R3−R5 and R3−R4, respectively. Dashed and dashed−dotted lines correspond to interactions between regions R4−R5 and R1−R2, respectively.

Table 3. Summary of the Main Changes in the Contact Map due to the Solvent[a]

	R1−R2	R1−R5	R3−R4	R3−R5	R4−R5
water	—	—	—	—	—
NaCl	↑	—	↓	↑	—
inositol	↑	↓	↓	↓	↑
4AP	—	—	↑	↓	↑

[a]Regions R1−R5 are defined in Figure 4. Upwards (↑) and downwards (↓) arrows represent an increase and decrease in the number of contacts between Aβ_{42} regions computed with respect to pure water (—).

Hydrogen Bonding Regions. Antiparallel contacts in Figure 5 suggest the existence of antiparallel β-hairpins in the structure of Aβ wherein strands are held together through backbone hydrogen bonds. In Figure 6a, regions R1−R5 are represented as vertices of a pentagon and the thickness of the lines connecting these vertices is proportional to the average number of hydrogen bonds between the different regions in pure water. More than two hydrogen bonds are formed on average between regions R1−R2 and R3−R4 (thick line), and more than one hydrogen bond is formed between R2−R3 (thin line). Added to the knowledge that regions R1, R2, R3, and R4 have a high probability to form strands (see Figure 4) and that regions R1−R2 as well as R3−R4 have a high

https://dx.doi.org/10.1021/acs.jpcb.0c09617
J. Phys. Chem. B 2021, 125, 1085−1097

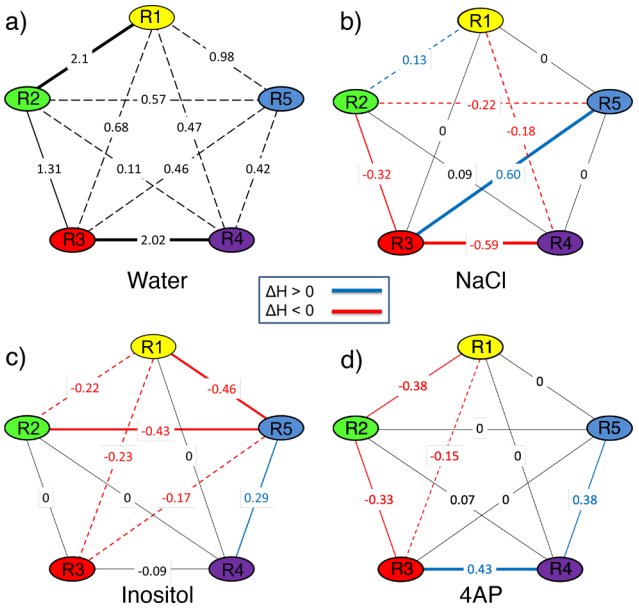

Figure 6. Hydrogen bond analysis. Regions R1−R5 are represented as vertices of a pentagon. (a) Thick, thin, and dashed lines are used to connect two vertices when the average number of hydrogen bonds between the corresponding regions is greater than 2, 1, or less than 1, respectively. Lines represent changes in the average number of hydrogen bonds compared to pure water for (b) NaCl, (c) inositol, and (d) 4AP. Blue and red lines are used to represent an increase and a decrease in the average number of hydrogen bonds relative to pure water simulation. Dashed, thin, and thick lines are used to represent changes in the magnitude of the number of hydrogen bonds that are less than 0.29, between 0.29 and 0.4, and more than 0.4, respectively.

probability to form antiparallel contacts (see Figure 5), this suggests the existence of β-hairpins or strand−loop−strand conformations between R1−R2 and R3−R4. Strand−loop−strand conformations, also called U-shaped structures, between R3−R4 have been observed and discussed in other computational studies[44,92,93] wherein the central hydrophobic core (mainly residues 16−22) and residues at the beginning of the C-terminus (residues 29−35) account for the two strands with the loop region comprising residues 23−28. A hairpin between regions R2−R3 may also be present in our simulations, although the contact map in pure water does not show significant amounts of antiparallel contacts—see Figure 5.

Compared to pure water simulations, changes in the average number of hydrogen bonds due to the presence of solutes are shown in Figure 6b−d. Red and blue lines are used to represent a reduction and an increase, respectively, in the average number of hydrogen bonds. The numbers of hydrogen bonds between regions R3−R4 and R3−R5 are reduced and increased, respectively, in the NaCl solution. This is consistent with changes in the frequency of contacts in Figure 5 as well as the increase in β-sheet content at the C-terminus in Figure 4. It suggests a shift in registry of the strand−loop−strand conformation wherein region R3 in the NaCl solution prefers to interact with the end, instead of the beginning, of the C-terminus. Strengthening of contacts through backbone hydrogen bonds is also observed between regions R1 and R2 in the NaCl solution. This is consistent with the formation of a β-hairpin, as suggested by contact maps in Figure 5, and increased β/turn content in these regions, Figure 4. The number of hydrogen bonds between most pairs of regions is reduced in the solution containing inositol consistent with an overall increase in disorder of the Aβ_{42} structure. In this solution, the number of hydrogen bonds only increases between regions R4 and R5. Similar effects on the Aβ_{42} structure are also observed in the presence of 4AP, except that in this solution the average number of hydrogen bonds shows a large increase between regions R3 and R4.

In summary, antagonistic effects of NaCl and inhibitors with respect to the number of hydrogen bonds are observed in regions R3−R5 and R4−R5. NaCl increases bonding between regions R3 and R5, whereas inhibitors increase bonding in regions R4−R5. Notice, however, that the absolute number of hydrogen bonds between the different regions is small, suggesting that the formation of tertiary Aβ_{42} structures, e.g., strand−loop−strand conformations, is transient.

Cluster Analysis. To gain insights into the diversity of Aβ_{42} conformations sampled in the different solutions, we use the gromos method, implemented in the GROMACS software package, with a RMSD cutoff of 3.5 Å for backbone atoms to group structures into clusters.[86] Representative structures of the five top clusters in each simulation setup are shown in Figure 7. Clusters are labeled S1−S5, and the percentage of structures that belong to each cluster is also shown in the figure. The top 5 and 10 clusters encompass approximately 25 and 40%, respectively, of all structures in the production run. Structures in Figure 7 differ significantly from each other, which highlights their transient nature in the simulation. Most residues in these structures form β-sheets and coil structures, and only a few form α-helices. Table 4 shows all of the clusters with β-sheets between selected pairs of regions R1−R5 defined in Figure 4. This table also depicts the percentage of conformations, within the top 5 clusters, that exhibit that particular β-sheet. This number is computed by adding the percentage of each cluster that forms the β-sheet of interest (given in Figure 7) divided by the added percentage of all top 5 clusters.

In pure water, more than 40% of the structures in the top 5 clusters form β-sheets between regions R1−R2 and R1−R5—see Table 4. This high percentage is consistent with the large average number of hydrogen bonds (i.e., 2.1 and 0.98, respectively) formed between these regions in the production run of the simulation—see Figure 6a. Also, 40% of the structures in the top 5 clusters exhibit a β-sheet between regions R3 and R5, whereas only a small number of hydrogen bonds (i.e., 0.46) are formed between these regions when computed over the whole production run—see Figure 6a. This suggests that R3−R5 β-sheets are over-represented in the top 5 clusters, whereas the opposite is expected for β-sheets between regions R3 and R4, which are under-represented in the top 5 clusters. In particular, the formation of R3−R4 β-sheets occurs with a percentage of only 15% in the top 5 clusters, whereas the computed number of hydrogen bonds (i.e., 2.02) between these regions over the whole production run is one of the largest ones—see Figure 6a. This calls for some caution when considering cluster analysis of the top 5 clusters, as they may not be fully representative of all of the conformations formed in the production run of the simulation. Nevertheless, it does prove useful to interpret Figure 7 quantitatively.

The top 5 clusters in Figure 7 show the important role played by NaCl and inositol/4AP on the formation of strand−loop−strand structures involving regions R3, R4, and R5 of Aβ. Inositol (see clusters S2, S4, and S5) and 4AP (see clusters S2, S3, S4, and S5) favor structures in which region R4 adopts a strand-like structure that can form β-sheets with regions R3

https://dx.doi.org/10.1021/acs.jpcb.0c09617
J. Phys. Chem. B 2021, 125, 1085−1097

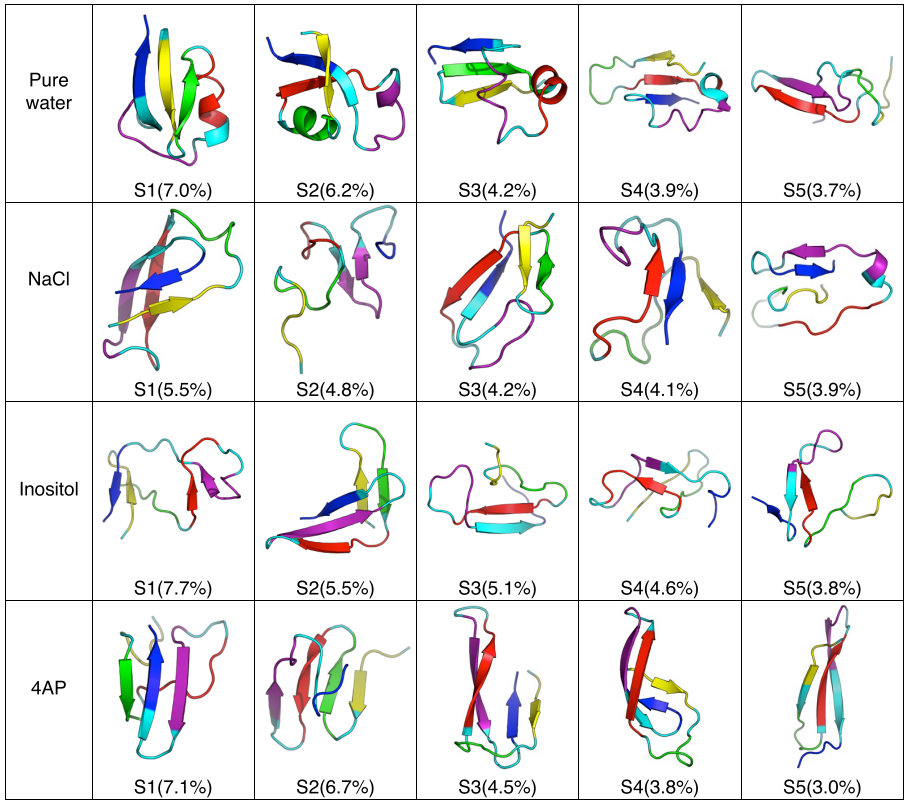

Figure 7. Representative structures of the five most populated clusters for the different solutions. For each solution, clusters are labeled S1−S5 and their population in percentage is given within parentheses. A color scheme based on Figure 4 is used: *yellow* for region R1 (residues 2−6), *green* for region 2 (residues 9−14), *red* for region 3 (residues 16−22), *purple* for region 4 (residues 26−32), *blue* for region 5 (residues 38−42), and *cyan* for all other residues.

Table 4. Diversity of the β-Sheets Formed in the Top 5 Clusters[a]

	R1−R2	R1−R5	R2−R5	R3−R4	R3−R5	R4−R5
water	S1, S3	S1, S2	S3	S5	S2, S4	
	44%	52%	17%	15%	40%	
NaCl	S3	S1, S4	S1	S1	S3, S4	S5
	18%	43%	24%	24%	37%	17%
inositol	S2	S1		S1, S2, S4, S5		S2, S5
	20%	29%		81%		35%
4AP	S2	S3, S4		S4, S3, S5	S2	S1, S3, S4
	27%	33%		45%	27%	61%

[a]Regions R1−R5 are defined in Figure 4, and clusters S1−S5 are depicted in Figure 7. The percentage of structures in the top 5 clusters with β-sheets between pairs of regions R*i*−R*j* is shown.

and/or R5. NaCl favors structures in which region R4 is part of the loop region that connects strands formed by regions R3 and R5—see clusters S2, S3, and S4 in Figure 7. These two set of structures are schematically represented in Figure 8, and they are consistent with Table 4 wherein the most frequent β-sheets in the top 5 clusters are found between regions R3−R4 and R4−R5 for inositol and 4AP and between regions R1−R5 and R3−R5 for NaCl. Structures in Figure 8 are also consistent with antagonistic effects of NaCl and inhibitors in regions R3−R5 and R4−R5, as discussed with respect to their frequency of contacts in Figure 5 and hydrogen bond analysis in Figure 6.

Strand−Loop−Strand Conformations. In our simulations, inhibitors promote conformations in which region R4 adopts a strand-like structure that forms β-sheets *with* regions R3 and/or R5—see Figure 8a. In contrast, NaCl favors conformations in which region R4 adopts a looplike structure, which enables the formation of an antiparallel β-sheet *between* regions R3 and R5, i.e., strand−loop−strand conformation—see Figure 8b. This is consistent with experimental studies suggesting that the formation of turns within residues 24−30 (which include most residues of region R4) constitutes an early folding event of Aβ fibril nucleation.[94−96] However, other studies also indicate that β-turn intermediates close to region R4 are not strictly required for Aβ fibril formation.[97,98]

In the strand−loop−strand structures promoted by NaCl, the close proximity of residues in regions R3 and R5 is consistent with the proximity of side chains stacked within the core of an NMR-derived fibril structure of Aβ_{42}, i.e., PDB ID 2BEG.[20] This structure is depicted in Figure 8b. Thus, the strand−loop−strand structure that is promoted in NaCl (Figure 8b) may constitute an intermediate structure on the pathway to fibril formation. This process would require the

https://dx.doi.org/10.1021/acs.jpcb.0c09617
J. Phys. Chem. B 2021, 125, 1085−1097

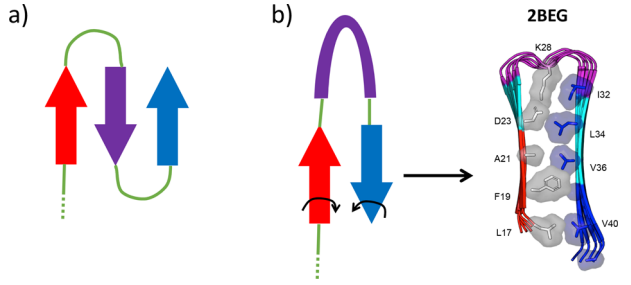

Figure 8. Schematic representations of strand−loop−strand structures that are promoted by (a) inhibitors and (b) NaCl. Red, purple, and blue colors are used to represent the central hydrophobic core (region R3), the central hydrophilic core (region R4), and the end of the C-terminus (region R5), respectively. The Venetian blind mechanism that may account for the nucleation of the 2BEG fibrils requires rotation of red and blue strands in panel b, as shown by black curved arrows.

two strands to rotate by an angle of 90°, as indicated by arrows in the figure. The energetic cost of rupturing the intrabackone hydrogen bonds in the strand−loop−strand structure would be compensated by the formation of new interpeptide hydrogen bonds in the fibril state. These strand-rotations could explain how antiparallel β-sheets formed in the monomeric state of Aβ_{42} nucleate into fibrils made of parallel β-sheets, as observed experimentally.[46,47] This mechanism by which fibril nucleation is preceded by the rotation of strands is known as the *Venetian blind* mechanism.[13,95]

Cluster S4 of the NaCl solution provides an example of the strand−loop−strand structure wherein regions R3 and R5 from an antiparallel β-sheet and region R4 adopts a loop-like structure. The population of conformations with similar structural characteristics in the different solutions is estimated in Figure 9 wherein we show RMSD distributions of Aβ_{42} conformations computed with respect to the S4 cluster of NaCl. The number of conformations with a structure comparable to the S4 cluster of NaCl, i.e., structures with RMSD $\leq$ 0.25 nm, is zero and small for aqueous solutions containing 4AP and inositol, respectively. In pure water and NaCl solution, structures that resemble the S4 cluster are more

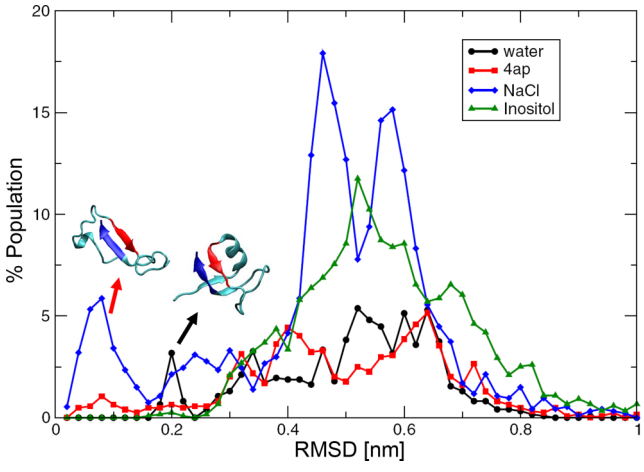

Figure 9. RMSD distributions of Aβ_{42} conformations in the production run computed with respect to the S4 cluster of NaCl. The RMSD is computed for C_α atoms of residues in regions R3 and R5. Representative structures with RMSD $\leq$ 0.25 nm for NaCl and pure water solutions are shown.

numerous, as they are represented by small and large peaks in the RMSD distribution. This leads us to speculate about a potential mechanism of fibril inhibition which involves discouraging structures that resemble the S4 cluster in NaCl.

IV. CONCLUSION

Effects of the aqueous solution on the structures sampled by Aβ_{42} monomers were studied using all-atom REMD simulations in explicit solvent. Consistent with other studies, we find that these structures are characterized by a high level of disorder with β-strands and turns forming along the peptide sequence.[13,41] Interactions between strands lead to the formation of transient antiparallel β-sheets that account for structures that are more compact than expected for a completely disordered protein made of 42 residues.[51] In pure water, most of these β-sheets occur between the central hydrophobic core and the central hydrophilic core of the protein as well as within segments of the N-terminus.[41,49,52]

Inositol and 4AP, which where shown to inhibit fibril formation in experiments, bind strongly to Aβ_{42} in a nonspecific manner. However, this does not have a strong effect on the secondary structure content of Aβ_{42}, except at the C-terminus, where β-sheets are discouraged in the presence of inositol, and at the central hydrophilic core, where β-sheets are favored in the presence of 4AP—see Figure 4a,b. Conversely, NaCl, which promotes fibril formation by reducing the lag phase in experiments, favors the formation of β-sheets at the N- and C-terminus while inhibiting β-sheets at the central hydrophilic core—see Figure 4a,b. This highlights antagonistic effects of NaCl and inhibitors on the structure of the C-terminus and central hydrophilic core. The C-terminus is less rigid in solutions containing NaCl—see Figure 4c. Moreover, NaCl and inhibitors promote binding of the C-terminus to different residues of Aβ_{42}. In NaCl, conformations in which the end of the C-terminus binds more frequently to the central hydrophobic core of the protein (region R3) are sampled more frequently compared to simulations performed in pure water—see Figure 8b. In inositol and 4AP solutions, the C-terminus binds less frequently to the central hydrophobic core and more frequently to the central hydrophilic core (region R4)—see Figure 8a. These results suggest a prominent role of the C-terminus in initiating aggregation which is supported by the increased rate of aggregation of Aβ_{42} compared to Aβ sequences with a shorter C-terminus.[10,34] This is also supported by biochemical experiments in which mutations of the C-terminus with poly-Q sequences were used to unravel the amyloidogenic potential of Aβ.[99]

In agreement with other computational studies, strands forming β-sheets in our simulations are linked to each other by a loop.[44] These strand−loop−strand structures have been shown to facilitate peptide addition to fibrils in coarse-grained models,[100] and they were proposed to be intermediate conformations on the pathway to fibril formation.[44] We show that the hydrogen bond registry of these structures is different in NaCl solution wherein side chains that form the hydrophobic core of the 2BEG fibril structure are in close proximity. The existence of such structures can facilitate fibril nucleation via a Venetian blind mechanism whereby strand rotation can lead to the formation of interpeptide hydrogen bonds seen in the 2BEG fibril—see Figure 8b. These strand−loop−strand structures are sampled in NaCl and pure water solutions but not in inositol and 4AP solutions.

https://dx.doi.org/10.1021/acs.jpcb.0c09617
J. Phys. Chem. B 2021, 125, 1085−1097

Despite the insights brought up by our study, its limitations should also be noted. We have chosen the AMBER99SB-ILDN force field and the TIP3P water model to carry out our simulations because of their proven record in reproducing several experimental quantities of proteins.[82,83] For the Aβ protein, this force field was shown to reproduce *J*-coupling coefficients obtained using NMR experiments.[13,41,51] This analysis is reproduced in the Supporting Information using configurations from our simulations showing similar agreement with experiments (see section S5 and Figure S10). Further investigations using different force fields are, however, necessary to provide an understanding of biases introduced by the different mathematical models. The extensive computational resources needed for that purpose (more than ∼45 μs per force field per aqueous solution) have stopped us from accomplishing this task. In addition, it is also desirable to study a broader set of small compounds to understand the universality of strand−loop−strand conformations and identify other possible structures that may promote Aβ_{42} aggregation. In this study, we have focused our attention on three molecules for which experimental evidence was available.[8,15,17,72,101] At last, we anticipate that faster computers will enable equilibrium conformations of Aβ aggregates to be studied in the near future.[50] This will allow strand−loop−strand structures in aggregates to be identified and compared to the ones pinpointed in this study as well as conformational changes leading to amyloid fibril formations, e.g., the *Venetian* blind mechanism.

■ ASSOCIATED CONTENT

Supporting Information

The Supporting Information is available free of charge at https://pubs.acs.org/doi/10.1021/acs.jpcb.0c09617.

Additional information about convergence of our simulations, force field parameters, secondary structure content, small molecules binding to Aβ monomers, and comparison of MD-derived $^3J_{HNHA}$ values with experiments (PDF)

■ AUTHOR INFORMATION

Corresponding Author

Cristiano L. Dias − *Department of Physics, New Jersey Institute of Technology, Newark, New Jersey 07102-1982, United States;* orcid.org/0000-0002-8765-3922; Email: cld@njit.edu

Authors

Farbod Mahmoudinobar − *Department of Physics, New Jersey Institute of Technology, Newark, New Jersey 07102-1982, United States;* orcid.org/0000-0002-4647-598X

Bradley L. Nilsson − *Department of Chemistry, University of Rochester, Rochester, New York 14627, United States;* orcid.org/0000-0003-1193-3693

Complete contact information is available at: https://pubs.acs.org/10.1021/acs.jpcb.0c09617

Notes

The authors declare no competing financial interest.

■ ACKNOWLEDGMENTS

This material is based upon the work supported by the National Science Foundation under Grant Nos. CHE-1904364 and CHE-1904528. Computational resources were provided by Compute Canada and the High Performance Computing Center at the New Jersey Institute of Technology.

■ REFERENCES

(1) Alzheimer, A. Über eigenartige krankheitsfälle des späteren alters. *Z. Gesamte Neurol. Psychiatr.* **1911**, *4* (1), 356−385.

(2) Alzheimer, A.; Forstl, H.; Levy, R. On certain peculiar diseases of old age. *Hist. Psychiatry* **1991**, *2* (5), 71−73.

(3) Hardy, J.; Higgins, G. Alzheimer's disease: the amyloid cascade hypothesis. *Science* **1992**, *256* (5054), 184−185.

(4) Nasica-Labouze, J.; Nguyen, P. H.; Sterpone, F.; Berthoumieu, O.; Buchete, N.-V.; Cote, S.; De Simone, A.; Doig, A. J.; Faller, P.; Garcia, A.; et al. Amyloid β protein and alzheimer's disease: When computer simulations complement experimental studies. *Chem. Rev.* **2015**, *115* (9), 3518−3563.

(5) Owen, M. C.; Gnutt, D.; Gao, M.; Warmlander, S. K. T. S.; Jarvet, J.; Graslund, A.; Winter, R.; Ebbinghaus, S.; Strodel, B. Effects of in vivo conditions on amyloid aggregation. *Chem. Soc. Rev.* **2019**, *48* (14), 3946−3996.

(6) Hatami, A.; Monjazeb, S.; Milton, S.; Glabe, C. G. Familial alzheimer's disease mutations within the amyloid precursor protein alter the aggregation and conformation of the amyloid-β peptide. *J. Biol. Chem.* **2017**, *292* (8), 3172−3185.

(7) Seeliger, J.; Estel, K.; Erwin, N.; Winter, R. Cosolvent effects on the fibrillation reaction of human iapp. *Phys. Chem. Chem. Phys.* **2013**, *15* (23), 8902−8907.

(8) Abelein, A.; Jarvet, J.; Barth, A.; Graslund, A.; Danielsson, J. Ionic strength modulation of the free energy landscape of aβ40 peptide fibril formation. *J. Am. Chem. Soc.* **2016**, *138* (21), 6893−6902.

(9) McLaurin, J.; Yang, D.-S.; Yip, C. M.; Fraser, P. E. Modulating factors in amyloid-β fibril formation. *J. Struct. Biol.* **2000**, *130* (2−3), 259−270.

(10) Murakami, K.; Irie, K.; Morimoto, A.; Ohigashi, H.; Shindo, M.; Nagao, M.; Shimizu, T.; Shirasawa, T. Neurotoxicity and physicochemical properties of aβ mutant peptides from cerebral amyloid angiopathy implication for the pathogenesis of cerebral amyloid angiopathy and alzheimer's disease. *J. Biol. Chem.* **2003**, *278* (46), 46179−46187.

(11) Benilova, I.; Gallardo, R.; Ungureanu, A. A.; Cano, V. C.; Snellinx, A.; Ramakers, M.; Bartic, C.; Rousseau, F.; Schymkowitz, J.; De Strooper, B. The alzheimer disease protective mutation a2t modulates kinetic and thermodynamic properties of amyloid-β (aβ) aggregation. *J. Biol. Chem.* **2014**, *289*, 30977−30989.

(12) Jonsson, T.; Atwal, J. K.; Steinberg, S.; Snaedal, J.; Jonsson, P. V.; Bjornsson, S.; Stefansson, H.; Sulem, P.; Gudbjartsson, D.; Maloney, J.; et al. A mutation in app protects against alzheimers disease and agerelated cognitive decline. *Nature* **2012**, *488* (7409), 96.

(13) Rosenman, D. J.; Wang, C.; Garcia, A. E. Characterization of Aβ Monomers through the Convergence of Ensemble Properties among Simulations with Multiple Force Fields. *J. Phys. Chem. B* **2016**, *120* (2), 259−277.

(14) Li, M. S.; Co, N. T.; Reddy, G.; Hu, C.-K.; Straub, J. E.; Thirumalai, D.; et al. Factors governing fibrillogenesis of polypeptide chains revealed by lattice models. *Phys. Rev. Lett.* **2010**, *105* (21), 218101.

(15) Felice, F. G.; Vieira, M. N. N.; Saraiva, L. M.; Figueroa-Villar, J. D.; Garcia-Abreu, J.; Liu, R.; Chang, L.; Klein, W. L.; Ferreira, S. T. Targeting the neurotoxic species in alzheimeras disease: inhibitors of aβ oligomerization. *FASEB J.* **2004**, *18* (12), 1366−1372.

(16) McLaurin, J.; Golomb, R.; Jurewicz, A.; Antel, J. P.; Fraser, P. E. Inositol stereoisomers stabilize an oligomeric aggregate of alzheimer amyloid β peptide and inhibit aβ-induced toxicity. *J. Biol. Chem.* **2000**, *275* (24), 18495−18502.

(17) McLaurin, J.; Franklin, T.; Chakrabartty, A.; Fraser, P. E. Phosphatidylinositol and inositol involvement in alzheimer amyloid-β fibril growth and arrest. *J. Mol. Biol.* **1998**, *278* (1), 183−194.

(18) Li, G.; Rauscher, S.; Baud, S.; Pomes, R. Binding of inositol stereoisomers to model amyloidogenic peptides. *J. Phys. Chem. B* **2012**, *116* (3), 1111−1119.
(19) Li, G.; Pomes, R. Binding mechanism of inositol stereoisomers to monomers and aggregates of aβ (16−22). *J. Phys. Chem. B* **2013**, *117* (22), 6603−6613.
(20) Luhrs, T.; Ritter, C.; Adrian, M.; Riek-Loher, D.; Bohrmann, B.; Dobeli, H.; Schubert, D.; Riek, R. 3d structure of alzheimeras amyloid-β (1−42) fibrils. *Proc. Natl. Acad. Sci. U. S. A.* **2005**, *102* (48), 17342−17347.
(21) Chen, W.-T.; Hong, C.-J.; Lin, Y.-T.; Chang, W.-H.; Huang, H.-T.; Liao, J.-Y.; Chang, Y.-J.; Hsieh, Y.-F.; Cheng, C.-Y.; Liu, H.-C.; et al. Amyloid-beta (aβ) d7h mutation increases oligomeric aβ42 and alters properties of aβ-zinc/copper assemblies. *PLoS One* **2012**, *7* (4), e35807.
(22) Zhou, L.; Brouwers, N.; Benilova, I.; Vandersteen, A.; Mercken, M.; Van Laere, K.; Van Damme, P.; Demedts, D.; Van Leuven, F.; Sleegers, K.; et al. Amyloid precursor protein mutation e682k at the alternative β-secretase cleavage β?-site increases aβ generation. *EMBO Mol. Med.* **2011**, *3* (5), 291−302.
(23) Kaden, D.; Harmeier, A.; Weise, C.; Munter, L. M.; Althoff, V.; Rost, B. R.; Hildebrand, P. W.; Schmitz, D.; Schaefer, M.; Lurz, R.; et al. Novel app/aβ mutation k16n produces highly toxic heteromeric aβ oligomers. *EMBO Mol. Med.* **2012**, *4* (7), 647−659.
(24) Hendriks, L.; van Duijn, C. M.; Cras, P.; Cruts, M.; Van Hul, W.; van Harskamp, F.; Warren, A.; McInnis, M. G.; Antonarakis, S. E.; Martin, J.-J.; et al. Presenile dementia and cerebral haemorrhage linked to a mutation at codon 692 of the β-amyloid precursor protein gene. *Nat. Genet.* **1992**, *1* (3), 218.
(25) Cras, P.; van Harskamp, F.; Hendriks, L.; Ceuterick, C.; van Duijn, C. M.; Stefanko, S. Z.; Hofman, A.; Kros, J. M.; Van Broeckhoven, C.; Martin, J. J.; van Harskamp, F. Presenile alzheimer dementia characterized by amyloid angiopathy and large amyloid core type senile plaques in the app 692ala-gly mutation. *Acta Neuropathol.* **1998**, *96* (3), 253−260.
(26) Nilsberth, C.; Westlind-Danielsson, A.; Eckman, C. B.; Condron, M. M.; Axelman, K.; Forsell, C.; Stenh, C.; Luthman, J.; Teplow, D. B.; Younkin, S. G.; et al. The arctic app mutation (e693g) causes alzheimer's disease by enhanced aβ protofibril formation. *Nat. Neurosci.* **2001**, *4* (9), 887.
(27) Obici, L.; Demarchi, A.; de Rosa, G.; Bellotti, V.; Marciano, S.; Donadei, S.; Arbustini, E.; Palladini, G.; Diegoli, M.; Genovese, E.; et al. A novel aβpp mutation exclusively associated with cerebral amyloid angiopathy. *Ann. Neurol.* **2005**, *58* (4), 639−644.
(28) Rossi, G.; Giaccone, G.; Maletta, R.; Morbin, M.; Capobianco, R.; Mangieri, M.; Giovagnoli, A. R.; Bizzi, A.; Tomaino, C.; Perri, M.; et al. A family with alzheimer disease and strokes associated with a713t mutation of the app gene. *Neurology* **2004**, *63* (5), 910−912.
(29) Armstrong, J.; Boada, M.; Rey, M. J.; Vidal, N.; Ferrer, I. Familial alzheimer disease associated with a713t mutation in app. *Neurosci. Lett.* **2004**, *370* (2−3), 241−243.
(30) Seubert, P.; Vigo-Pelfrey, C.; Esch, F.; Lee, M.; Dovey, H.; Davis, D.; Sinha, S.; Schiossmacher, M.; Whaley, J.; Swindlehurst, C.; et al. Isolation and quantification of soluble alzheimeras β-peptide from biological fluids. *Nature* **1992**, *359* (6393), 325−327.
(31) Gravina, S. A.; Ho, L.; Eckman, C. B.; Long, K. E.; Otvos, L.; Younkin, L. H.; Suzuki, N.; Younkin, S. G. Amyloid β protein (aβ) in alzheimer's disease brain biochemical and immunocytochemical analysis with antibodies specific for forms ending at aβ40 or aβ42 (43). *J. Biol. Chem.* **1995**, *270* (13), 7013−7016.
(32) Näslund, J.; Haroutunian, V.; Mohs, R.; Davis, K. L.; Davies, P.; Greengard, P.; Buxbaum, J. D. Correlation between elevated levels of amyloid β-peptide in the brain and cognitive decline. *JAMA* **2000**, *283* (12), 1571−1577.
(33) Roberts, B. R.; Lind, M.; Wagen, A. Z.; Rembach, A.; Frugier, T.; Li, Q.-X.; Ryan, T. M.; McLean, C. A.; Doecke, J. D.; Rowe, C. C.; et al. Biochemically-defined pools of amyloid-β in sporadic alzheimeras disease: correlation with amyloid pet. *Brain* **2017**, *140* (5), 1486−1498.
(34) Haass, C.; Selkoe, D. J. Soluble protein oligomers in neurodegeneration: lessons from the alzheimeras amyloid β-peptide. *Nat. Rev. Mol. Cell Biol.* **2007**, *8* (2), 101−112.
(35) Jarrett, J. T.; Berger, E. P.; Lansbury, P. T. The carboxy terminus of the. beta. amyloid protein is critical for the seeding of amyloid formation: Implications for the pathogenesis of alzheimeras disease. *Biochemistry* **1993**, *32* (18), 4693−4697.
(36) Aleksis, R.; Oleskovs, F.; Jaudzems, K.; Pahnke, J.; Biverstal, H. Structural studies of amyloid-β peptides: Unlocking the mechanism of aggregation and the associated toxicity. *Biochimie* **2017**, *140*, 176−192.
(37) Ball, K. A.; Phillips, A. H.; Nerenberg, P. S.; Fawzi, N. L.; Wemmer, D. E.; Head-Gordon, T. Homogeneous and heterogeneous tertiary structure ensembles of amyloid-β peptides. *Biochemistry* **2011**, *50* (35), 7612−7628.
(38) Morel, B.; Conejero-Lara, F. Early mechanisms of amyloid fibril nucleation in model and disease-related proteins. *Biochim. Biophys. Acta, Proteins Proteomics* **2019**, *1867*, 140264.
(39) Roche, J.; Shen, Y.; Lee, J. H.; Ying, J.; Bax, A. Monomeric aβ1−40 and aβ1−42 peptides in solution adopt very similar ramachandran map distributions that closely resemble random coil. *Biochemistry* **2016**, *55* (5), 762−775.
(40) Nag, S.; Sarkar, B.; Bandyopadhyay, A.; Sahoo, B.; Sreenivasan, V. K. A.; Kombrabail, M.; Muralidharan, C.; Maiti, S. Nature of the amyloid-β monomer and the monomer-oligomer equilibrium. *J. Biol. Chem.* **2011**, *286* (16), 13827−13833.
(41) Rosenman, D. J.; Connors, C. R.; Chen, W.; Wang, C.; Garcia, A. E. Aβ monomers transiently sample oligomer and fibril-like configurations: Ensemble characterization using a combined MD/NMR approach. *J. Mol. Biol.* **2013**, *425* (18), 3338−3359.
(42) Hou, L.; Shao, H.; Zhang, Y.; Li, H.; Menon, N. K.; Neuhaus, E. B.; Brewer, J. M.; Byeon, I.-J. L.; Ray, D. G.; Vitek, M. P.; et al. Solution nmr studies of the aβ (1- 40) and aβ (1- 42) peptides establish that the met35 oxidation state affects the mechanism of amyloid formation. *J. Am. Chem. Soc.* **2004**, *126* (7), 1992−2005.
(43) Walti, M. A.; Orts, J.; Vogeli, B.; Campioni, S.; Riek, R. Solution nmr studies of recombinant aβ (1−42): From the presence of a micellar entity to residual β-sheet structure in the soluble species. *ChemBioChem* **2015**, *16* (4), 659−669.
(44) Han, W.; Wu, Y.-D. A strand-loop-strand structure is a possible intermediate in fibril elongation: Long time simulations of amyloid-β peptide (10- 35). *J. Am. Chem. Soc.* **2005**, *127* (44), 15408−15416.
(45) Ono, K.; Condron, M. M.; Teplow, D. B. Structure-neurotoxicity relationships of amyloid β-protein oligomers. *Proc. Natl. Acad. Sci. U. S. A.* **2009**, *106* (35), 14745−14750.
(46) Cerf, E.; Sarroukh, R.; Tamamizu-Kato, S.; Breydo, L.; Derclaye, S.; Dufrene, Y. F.; Narayanaswami, V.; Goormaghtigh, E.; Ruysschaert, J.-M.; Raussens, V. Antiparallel β-sheet: a signature structure of the oligomeric amyloid β-peptide. *Biochem. J.* **2009**, *421* (3), 415−423.
(47) Sarroukh, R.; Goormaghtigh, E.; Ruysschaert, J.-M.; Raussens, V. Atr-ftir: a "rejuvenated" tool to investigate amyloid proteins. *Biochim. Biophys. Acta, Biomembr.* **2013**, *1828* (10), 2328−2338.
(48) Sgourakis, N. G.; Merced-Serrano, M.; Boutsidis, C.; Drineas, P.; Du, Z.; Wang, C.; Garcia, A. E. Atomic-level characterization of the ensemble of the aβ (1−42) monomer in water using unbiased molecular dynamics simulations and spectral algorithms. *J. Mol. Biol.* **2011**, *405* (2), 570−583.
(49) Cote, S.; Derreumaux, P.; Mousseau, N. Distinct morphologies for amyloid beta protein monomer: Aβ1−40, aβ1−42, and aβ1−40 (d23n). *J. Chem. Theory Comput.* **2011**, *7* (8), 2584−2592.
(50) Man, V. H.; Nguyen, P. H.; Derreumaux, P. High-resolution structures of the amyloid-β 1−42 dimers from the comparison of four atomistic force fields. *J. Phys. Chem. B* **2017**, *121* (24), 5977−5987.
(51) Carballo-Pacheco, M.; Strodel, B. Comparison of force fields for alzheimer's a: A case study for intrinsically disordered proteins. *Protein Sci.* **2017**, *26* (2), 174−185.

https://dx.doi.org/10.1021/acs.jpcb.0c09617
J. Phys. Chem. B 2021, 125, 1085−1097

(52) Yang, M.; Teplow, D. B. Amyloid β-protein monomer folding: free-energy surfaces reveal alloform-specific differences. *J. Mol. Biol.* **2008**, *384* (2), 450−464.
(53) Lim, K. H.; Collver, H. H.; Le, Y. T.H.; Nagchowdhuri, P.; Kenney, J. M. Characterizations of distinct amyloidogenic conformations of the aβ (1−40) and (1−42) peptides. *Biochem. Biophys. Res. Commun.* **2007**, *353* (2), 443−449.
(54) Yan, Y.; Wang, C. Aβ42 is more rigid than aβ40 at the c terminus: implications for aβ aggregation and toxicity. *J. Mol. Biol.* **2006**, *364* (5), 853−862.
(55) Velez-Vega, C.; Escobedo, F. A. Characterizing the structural behavior of selected aβ-42 monomers with different solubilities. *J. Phys. Chem. B* **2011**, *115* (17), 4900−4910.
(56) Das, P.; Murray, B.; Belfort, G. Alzheimer's protective a2t mutation changes the conformational landscape of the aβ1−42 monomer differently than does the a2v mutation. *Biophys. J.* **2015**, *108* (3), 738−747.
(57) Maloney, J. A.; Bainbridge, T.; Gustafson, A.; Zhang, S.; Kyauk, R.; Steiner, P.; van der Brug, M.; Liu, Y.; Ernst, J. A.; Watts, R. J.; et al. Molecular mechanisms of alzheimer disease protection by the a673t allele of amyloid precursor protein. *J. Biol. Chem.* **2014**, *289* (45), 30990−31000.
(58) Gaudreault, R.; Mousseau, N. Mitigating alzheimer's disease with natural polyphenols: a review. *Curr. Alzheimer Res.* **2019**, *16* (6), 529−543.
(59) Nie, Q.; Du, X.-g.; Geng, M.-y. Small molecule inhibitors of amyloid β peptide aggregation as a potential therapeutic strategy for alzheimer's disease. *Acta Pharmacol. Sin.* **2011**, *32* (5), 545−551.
(60) Hard, T.; Lendel, C. Inhibition of amyloid formation. *J. Mol. Biol.* **2012**, *421* (4−5), 441−465.
(61) Uversky, V. N.; Li, J.; Fink, A. L. Trimethylamine-n-oxide-induced folding of α-synuclein. *FEBS Lett.* **2001**, *509* (1), 31−35.
(62) Citron, M. Alzheimer's disease: strategies for disease modification. *Nat. Rev. Drug Discovery* **2010**, *9* (5), 387.
(63) Roberson, E. D.; Mucke, L. 100 years and counting: prospects for defeating alzheimeras disease. *Science* **2006**, *314* (5800), 781−784.
(64) Warmlander, S.; Tiiman, A.; Abelein, A.; Luo, J.; Jarvet, J.; Soderberg, K. L.; Danielsson, J.; Graslund, A. Biophysical studies of the amyloid β-peptide: Interactions with metal ions and small molecules. *ChemBioChem* **2013**, *14* (14), 1692−1704.
(65) Raman, E. P.; Takeda, T.; Klimov, D. K. Molecular dynamics simulations of ibuprofen binding to aβ peptides. *Biophys. J.* **2009**, *97* (7), 2070−2079.
(66) Lockhart, C.; Kim, S.; Klimov, D. K. Explicit solvent molecular dynamics simulations of aβ peptide interacting with ibuprofen ligands. *J. Phys. Chem. B* **2012**, *116* (43), 12922−12932.
(67) Ngo, S. T.; Li, M. S. Curcumin binds to aβ1−40 peptides and fibrils stronger than ibuprofen and naproxen. *J. Phys. Chem. B* **2012**, *116* (34), 10165−10175.
(68) Takeda, T.; Kumar, R.; Raman, E. P.; Klimov, D. K. Nonsteroidal anti-inflammatory drug naproxen destabilizes aβ amyloid fibrils: a molecular dynamics investigation. *J. Phys. Chem. B* **2010**, *114* (46), 15394−15402.
(69) Zou, Y.; Qian, Z.; Chen, Y.; Qian, H.; Wei, G.; Zhang, Q. Norepinephrine inhibits alzheimers amyloid-β peptide aggregation and destabilizes amyloid-β protofibrils: A molecular dynamics simulation study. *ACS Chem. Neurosci.* **2019**, *10* (3), 1585−1594.
(70) Fan, H.-M.; Gu, R.-X.; Wang, Y.-J.; Pi, Y.-L.; Zhang, Y.-H.; Xu, Q.; Wei, D.-Q. Destabilization of alzheimer's aβ42 protofibrils with a novel drug candidate wgx-50 by molecular dynamics simulations. *J. Phys. Chem. B* **2015**, *119* (34), 11196−11202.
(71) Bleiholder, C.; Do, T. D.; Wu, C.; Economou, N. J.; Bernstein, S. S.; Buratto, S. K.; Shea, J.-E.; Bowers, M. T. Ion mobility spectrometry reveals the mechanism of amyloid formation of aβ (25−35) and its modulation by inhibitors at the molecular level: epigallocatechin gallate and scyllo-inositol. *J. Am. Chem. Soc.* **2013**, *135* (45), 16926−16937.
(72) Sinha, S.; Du, Z.; Maiti, P.; Klarner, F.-G.; Schrader, T.; Wang, C.; Bitan, G. Comparison of three amyloid assembly inhibitors: the sugar scyllo-inositol, the polyphenol epigallocatechin gallate, and the molecular tweezer clr01. *ACS Chem. Neurosci.* **2012**, *3* (6), 451−458.
(73) Viles, J. H. Metal ions and amyloid fiber formation in neurodegenerative diseases. copper, zinc and iron in alzheimer's, parkinson's and prion diseases. *Coord. Chem. Rev.* **2012**, *256* (19−20), 2271−2284.
(74) Dong, J.; Atwood, C. S.; Anderson, V. E.; Siedlak, S. L.; Smith, M. A.; Perry, G.; Carey, P. R. Metal binding and oxidation of amyloid-β within isolated senile plaque cores: Raman microscopic evidence. *Biochemistry* **2003**, *42* (10), 2768−2773.
(75) Lovell, M. A.; Robertson, J. D.; Teesdale, W. J.; Campbell, J. L.; Markesbery, W. R. Copper, iron and zinc in alzheimer's disease senile plaques. *J. Neurol. Sci.* **1998**, *158* (1), 47−52.
(76) Miller, L. M.; Wang, Q.; Telivala, T. P.; Smith, R. J.; Lanzirotti, A.; Miklossy, J. Synchrotron-based infrared and x-ray imaging shows focalized accumulation of cu and zn co-localized with β-amyloid deposits in alzheimer's disease. *J. Struct. Biol.* **2006**, *155* (1), 30−37.
(77) Sharma, A.; Behrens, S. H.; Chernoff, Y. O.; Bommarius, A. S. Modulation of the formation of aβ-and sup35nm-based amyloids by complex interplay of specific and nonspecific ion effects. *J. Phys. Chem. B* **2018**, *122* (19), 4972−4981.
(78) Klement, K.; Wieligmann, K.; Meinhardt, J.; Hortschansky, P.; Richter, W.; Fandrich, M. Effect of different salt ions on the propensity of aggregation and on the structure of alzheimers aβ (1−40) amyloid fibrils. *J. Mol. Biol.* **2007**, *373* (5), 1321−1333.
(79) Viet, M. H.; Siposova, K.; Bednarikova, Z.; Antosova, A.; Nguyen, T. T.; Gazova, Z.; Li, M. S. In silico and in vitro study of binding affinity of tripeptides to amyloid β fibrils: Implications for alzheimer's disease. *J. Phys. Chem. B* **2015**, *119* (16), 5145−5155.
(80) Chakraborty, S.; Das, P. Emergence of alternative structures in amyloid beta 1−42 monomeric landscape by n-terminal hexapeptide amyloid inhibitors. *Sci. Rep.* **2017**, *7* (1), 9941.
(81) Crescenzi, O.; Tomaselli, S.; Guerrini, R.; Salvadori, S.; D'Ursi, A. M.; Temussi, P. A.; Picone, D. Solution structure of the alzheimer amyloid β-peptide (1−42) in an apolar microenvironment: Similarity with a virus fusion domain. *Eur. J. Biochem.* **2002**, *269* (22), 5642−5648.
(82) Piana, S.; Klepeis, J. L; Shaw, D. E Assessing the accuracy of physical models used in protein-folding simulations: quantitative evidence from long molecular dynamics simulations. *Curr. Opin. Struct. Biol.* **2014**, *24*, 98−105.
(83) Lindorff-Larsen, K.; Piana, S.; Palmo, K.; Maragakis, P.; Klepeis, J. L.; Dror, R. O.; Shaw, D. E. Improved side-chain torsion potentials for the Amber ff99SB protein force field. *Proteins: Struct., Funct., Genet.* **2010**, *78* (8), 1950−1958.
(84) Mahmoudinobar, F.; Urban, J. M.; Su, Z.; Nilsson, B. L.; Dias, C. L. Thermodynamic stability of polar and nonpolar amyloid fibrils. *J. Chem. Theory Comput.* **2019**, *15* (6), 3868−3874.
(85) Sugita, Y.; Okamoto, Y. Replica-exchange molecular dynamics method for protein folding. *Chem. Phys. Lett.* **1999**, *314* (1−2), 141−151.
(86) Abraham, M. J.; Murtola, T.; Schulz, R.; Pall, S.; Smith, J. C.; Hess, B.; Lindahl, E. Gromacs: High performance molecular simulations through multi-level parallelism from laptops to supercomputers. *SoftwareX* **2015**, *1-2*, 19−25.
(87) Patriksson, A.; van der Spoel, D. A temperature predictor for parallel tempering simulations. *Phys. Chem. Chem. Phys.* **2008**, *10* (15), 2073−2077.
(88) Joosten, R. P.; te Beek, T. A. H.; Krieger, E.; Hekkelman, M. L.; Hooft, R. W. W.; Schneider, R.; Sander, C.; Vriend, G. A series of pdb related databases for everyday needs. *Nucleic Acids Res.* **2011**, *39* (Suppl_1), D411−D419.
(89) Wang, J.; Wolf, R. M.; Caldwell, J. W.; Kollman, P. A.; Case, D. A. Development and testing of a general amber force field. *J. Comput. Chem.* **2004**, *25* (9), 1157−1174.
(90) Joung, I. S.; Cheatham, T. E. Determination of alkali and halide monovalent ion parameters for use in explicitly solvated biomolecular simulations. *J. Phys. Chem. B* **2008**, *112* (30), 9020−9041.

https://dx.doi.org/10.1021/acs.jpcb.0c09617
J. Phys. Chem. B 2021, 125, 1085−1097

(91) Kohn, J. E.; Millett, I. S.; Jacob, J.; Zagrovic, B.; Dillon, T. M.; Cingel, N.; Dothager, R. S.; Seifert, S.; Thiyagarajan, P.; Sosnick, T. R.; et al. Random-coil behavior and the dimensions of chemically unfolded proteins. *Proc. Natl. Acad. Sci. U. S. A.* **2004**, *101* (34), 12491−12496.
(92) Wu, C.; Murray, M. M.; Bernstein, S. L.; Condron, M. M.; Bitan, G.; Shea, J.-E.; Bowers, M. T. The structure of aβ42 c-terminal fragments probed by a combined experimental and theoretical study. *J. Mol. Biol.* **2009**, *387* (2), 492−501.
(93) Miller, Y.; Ma, B.; Nussinov, R. Polymorphism in alzheimer aβ amyloid organization reflects conformational selection in a rugged energy landscape. *Chem. Rev.* **2010**, *110* (8), 4820−4838.
(94) Lazo, N. D.; Grant, M. A.; Condron, M. C.; Rigby, A. C.; Teplow, D. B. On the nucleation of amyloid β-protein monomer folding. *Protein Sci.* **2005**, *14* (6), 1581−1596.
(95) Hoyer, W.; Gronwall, C.; Jonsson, A.; Stahl, S.; Hard, T. Stabilization of a β-hairpin in monomeric alzheimeras amyloid-β peptide inhibits amyloid formation. *Proc. Natl. Acad. Sci. U. S. A.* **2008**, *105* (13), 5099−5104.
(96) Sandberg, A.; Luheshi, L. M.; Sollvander, S.; Pereira de Barros, T.; Macao, B.; Knowles, T. P. J.; Biverstal, H.; Lendel, C.; Ekholm-Petterson, F.; Dubnovitsky, A.; et al. Stabilization of neurotoxic alzheimer amyloid-β oligomers by protein engineering. *Proc. Natl. Acad. Sci. U. S. A.* **2010**, *107* (35), 15595−15600.
(97) Doran, T. M.; Anderson, E. A.; Latchney, S. E.; Opanashuk, L. A.; Nilsson, B. L. An azobenzene photoswitch sheds light on turn nucleation in amyloid-β self-assembly. *ACS Chem. Neurosci.* **2012**, *3* (3), 211−220.
(98) Doran, T. M.; Anderson, E. A.; Latchney, S. E.; Opanashuk, L. A.; Nilsson, B. L. Turn nucleation perturbs amyloid β self-assembly and cytotoxicity. *J. Mol. Biol.* **2012**, *421* (2−3), 315−328.
(99) Misra, P.; Kodali, R.; Chemuru, S.; Kar, K.; Wetzel, R. Rapid α-oligomer formation mediated by the aβ c terminus initiates an amyloid assembly pathway. *Nat. Commun.* **2016**, *7* (1), 12419.
(100) Han, W.; Schulten, K. Fibril elongation by aβ17−42: Kinetic network analysis of hybrid-resolution molecular dynamics simulations. *J. Am. Chem. Soc.* **2014**, *136* (35), 12450−12460.
(101) McLaurin, J.; Kierstead, M. E; Brown, M. E; Hawkes, C. A; Lambermon, M. H L; Phinney, A. L; Darabie, A. A; Cousins, J. E; French, J. E; Lan, M. F; Chen, F.; Wong, S. S N; Mount, H. T J; Fraser, P. E; Westaway, D.; George-Hyslop, P. S. Cyclohexanehexol inhibitors of aβ aggregation prevent and reverse alzheimer phenotype in a mouse model. *Nat. Med.* **2006**, *12* (7), 801.

https://dx.doi.org/10.1021/acs.jpcb.0c09617
J. Phys. Chem. B 2021, 125, 1085−1097